UDK 546.46:57.012.3
Original scientific article/Izvirni znanstveni članek

ISSN 1580-2949
Mater. Tehnol.

INFLUENCE OF EXTRUSION TEMPERATURE AND COOLING RATE ON THE MICROSTRUCTURE AND MECHANICAL PROPERTIES OF PRE-AGED EXTRUDED ZK61 Mg ALLOY

VPLIV TEMPERATURE IZTISKOVANJA IN HITROSTI OHLAJANJA NA MEHANSKE LASTNOSTI PREDHODNO STARANE MAGNEZIJEVE ZLITINE ZK61

Jian Xu, Yong Xue, Liang Liu, Bin Liu

College of Materials Science and Engineering, North University of China, 3 Xueyuan Road, Taiyuan 030051, China

Prejem rokopisa – received: 2023-10-10; sprejem za objavo – accepted for publication: 2025-06-04

doi:10.17222/mit.2023.1025

Deformation temperature and cooling rate have a large influence on the microstructure and mechanical properties. In this paper, the effects of pre-ageing extrusion temperatures (240, 320) °C and subsequent cooling modes (air cooled, 27 °C water cooled) on the microstructure and mechanical properties of extruded ZK61 alloy were investigated. The microstructure evolution mechanisms as well as dynamic recrystallization (DRX) principle were explored, and the strength-plasticity mechanism was analyzed. The higher the extrusion temperature, the higher the DRX ratio, and the larger the grain size. A higher temperature also provides energy for grain-boundary migration. The faster the cooling rate, the fewer the precipitated phases, the lower the DRX fraction, and the finer the grain size. A faster cooling rate did not allow enough time for the precipitates to nucleate, and DRX grains did not have the time to grow. The 240 °C extruded and air-cooled (LA) sample showed the best strength-plasticity synergy, with ultimate tensile strength (UTS), yield strength (YS), and elongation (EL) of 359.7 MPa, 281.8 MPa, and 18.8 %, respectively. This was mainly the result of a combined effect of fine-grain strengthening, dislocation strengthening, and texture strengthening.

Keywords: ZK61 Mg alloys, extrusion, microstructure, mechanical properties

Temperatura deformacije in hitrost ohlajanja imata oba velik vpliv na mikrostrukturo in s tem posledično na mehanske lastnosti kovinskih materialov. V tem članku avtorji opisujejo raziskavo vpliva predhodno starane magnezijeve zlitine tipa ZK61, ki so jo nato vroče ekstrudirali (iztiskovali) pri temperaturah 240 °C in 320 °C. Po ekstrudiranju je sledilo takojšnje ohlajanje na dva načina (hlajenje na zraku in hlajenje z 27 °C vodo). Sledila je mikrostrukturna in mehanska karakterizacija izdelanih zlitin. Avtorji so analizirali razvoj mikrostrukture in mehanizme dinamične rekristalizacije (DRX). Višja je temperatura ekstruzije, večja je hitrost DRX in večja so kristalna zrna, saj je na razpolago več energije za migracijo kristalnih mej. Večja je hitrost ohlajanja po ekstruziji, manjši je delež izločkov sekundarnih faz, manjša je hitrost DRX in bolj drobna so kristalna zrna. Večja hitrost ohlajanja ne daje dovolj časa za nukleacijo izločkov (precipitatov) in DRX kristalna zrna nimajo časa rasti. Zlitina ekstrudirana pri 240 °C in potem ohlajana na zraku je imela najboljšo sinergijo med trdnostjo in plastičnostjo. Končna trdnost te zlitine je bila 359,7 MPa, meja plastičnosti 281,8 MPa in raztezek 18,8 %. To je bila v glavnem posledica kombiniranega učinka utrjevanja zaradi udrobljenja kristalnih zrn ter dislokacijskega in teksturnega utrjevanja.

Ključne besede: magnezijeva zlitina tipa ZK61, ekstruzija, mikrostruktura, mehanske lastnosti

1 INTRODUCTION

Magnesium (Mg) alloys are widely used in aerospace, military and transportation due to their low density (1.8 g/cm^3), excellent specific strength, and good vibration damping properties.[1–4] The high-strength Mg-RE alloys, which are commonly used nowadays, have received extensive attention from researchers and scholars due to their better solution-strengthening as well as precipitation-strengthening effects.[5–7] However, due to the high prices of RE elements, Mg-RE system alloys are costly and not suitable for large-scale industrial applications. The Mg-Zn-Zr magnesium alloy exhibits one of the best overall performance profiles among high-strength wrought Mg alloys. The Zn element mainly improves the strength through dispersive strengthening and solid solution strengthening, while the Zr element has a strong role in refining the grains, improving the corrosion resistance and mechanical properties.[8–10] In this study, ZK61 Mg alloy was chosen for its high strength and good plasticity. It meets the performance requirements of most structural components, and is also the most widely used wrought magnesium alloy for commercial applications due to its low cost.

The combination of deformation and heat treatment is an effective means of modifying an initial microstructure. Pre-ageing treatment refers to the aging of an alloy before deformation, while the precipitation of the second phase can affect the microstructure and mechanical properties during the subsequent deformation.[11–13] Mg-6Zn-1Gd-1Er alloys exhibit lower deformation activation energies during hot compression when they are subjected to pre-ageing.[14] The interaction between

*Corresponding author's e-mail:
yongxue395@163.com (Yong Xue)

pre-existing precipitates and dislocations promotes DRX behavior, making the pre-aged samples more favorable for DRX than the solid solution heat-treated samples.[15] The effect of second-phase particles produced during the pre-aging of ZK60 alloys on DRX behavior was analyzed. It was found that coarse particles distributed in grain boundaries accelerate grain-boundary nucleation. Coarse particles distributed in the grains had a significant particle-stimulated nucleation (PSN) effect, promoting the nucleation of DRX grains. Fine precipitates distributed at the new grain boundaries had a pinning effect on the migration of grain boundaries, preventing the growth of DRX grains.[15–17] In summary, pre-ageing improves grain refinement and mechanical properties. For this reason, our study investigated the aging treatment prior to deformation.

The technique of severe plastic deformation (SPD) refers to the introduction of a large strain into the deformation process. It effectively refines the microstructure, and improves the forming properties of Mg alloys. It mainly includes the following methods: equal channel angular pressing (ECAP), high pressure torsion deformation (HCP), multidirectional forging (MDF) and friction stir processing (FSP). Li et al.[18] employed FSP to refine the coarse LPSO phase in Mg-12.8Y-4.7Zn (*w*/%) alloy. The results showed that the coarse LPSO phase was refined into dense ultrafine needles with an average width of ≈200 nm and an average length of ≈1 μm. The results obtained by Wei et al.[19] showed that the yield strength, ultimate tensile strength and elongation of Mg-7Gd-2Y-1Zn-0.5Zr alloy after extrusion and MDF were 395.2 MPa, 435.3 MPa and 17.6 %, respectively. However, the disadvantages of the aforementioned process include the limited size of processed parts and the need for specialized equipment, restricting its industrial application. In order to overcome the above drawbacks, the traditional extrusion experiment was used in this study.

Extrusion is a process that has emerged and developed based on traditional forming processes, and it is currently widely applied. Its advantages include simple equipment and operational flexibility.[20–24] The microstructure and mechanical properties of an extruded alloy are closely related to the deformation parameters and cooling mode. Wang et al.[25] investigated the effects of different extrusion ratios and subsequent cooling processes on the microstructure, texture and mechanical properties of Mg-8Gd-4Y–1Zn–Mn (*w*/%) extruded alloys. The results showed that increasing the extrusion ratio promoted DRX, while water cooling inhibited static recrystallization (SRX) compared with air cooling. Decreasing the extrusion ratio or increasing the cooling rate leads to the formation of coarse, un-DRXed grains, and the effect of rapid cooling on the refinement of recrystallized grains is also obvious. Different extrusion conditions affect the mechanical properties of Mg-2Gd-0.3Zr alloys through the grain size, proportion of non-recrystallized zones and type of texture.[26] Therefore, in order to obtain high-strength ZK61 extrusion alloys, it is essential to investigate the effects of different extrusion temperatures and cooling rates on the microstructure and mechanical properties.

At present, the ZK61 alloy is typically extruded and deformed in a temperature range of 300–400 °C. The relationship between microstructure and mechanical properties was explored. This study mainly investigated the effects of low extrusion temperatures (240, 320) °C and different cooling rates (27 °C water cooling, air cooling) on the microstructure and mechanical properties of extruded alloys. An in-depth analysis of the DRX mechanism was carried out, investigating the specific effects of dynamic precipitation on the microstructure evolution and mechanical properties of extruded Mg alloys.

2 EXPERIMENTAL PART

In this study, experimental material was as-cast Mg-5.99Zn-0.98Zr (*w*/%) alloy billets (dimensions of $\phi 45 \times 60$ mm). The prepared billets were first homogenized in a resistance furnace at 415 °C for 16 h and then water quenched at room temperature (RT) and recorded as S samples. The homogenized specimens were subjected to aging treatment at 175 °C for 12 h followed by air cooling, and recorded as A samples. The billets were preheated at 320 °C for 40 min, and the extrusion die was held at 40 °C above the extrusion temperature for 8 h. The extrusion experiment was carried out at two temperatures (240, 320) °C with an extrusion ratio of 9:1 and an extrusion speed of 0.1 mm/s. The extruded specimens were cooled by 27°C water cooling and air cooling, respectively. Different treatment processes are summarized in **Table 1**.

A microstructure analysis of different specimens was carried out using optical microscopy (OM, Zeiss Axio ImagerA2 m) and scanning electron microscopy (SEM, Hitachi SU5000). First, the specimens were subjected to mechanical polishing (with water abrasive sandpaper of different roughness levels) and etching (1 g picric acid, 2 mL acetic acid, 14 mL alcohol and 2 mL distilled water), followed by photographic metallography using an OM. Electron backscatter diffraction (EBSD) experiments were carried out at an accelerating voltage of 20 kV, working distance of 15 mm and inclination angle of 70°. The results were post-processed using Orientation Imaging Microscopy (OIM) Analysis 7.0 software, obtained from EDAX.

Mechanical properties of different specimens were tested using an Instron-3382 with a strain rate of 8×10^{-3} mm/s at RT. Tensile tests of the specimens in different states were repeated three times, and the average values were taken to ensure accuracy. Hardness tests were carried out using a Vickers hardness machine (HV, UHL-VMHT) with a load of 200 g, holding time of 15 s. Measurements were taken at 20 points, and the average

value was calculated after excluding the maximum and minimum values.

Table 1: Extruded ZK61 Mg alloys in different states

Designation	Deformation parameters and cooling method
S sample	1. As-cast billet 2. 415 °C for 16 h
A sample	1. S sample 2. 175 °C for 12 h
LA sample	1. A sample 2. Hot extrusion (240 °C, 9:1) 3. Air cooling
HA sample	1. A sample 2. Hot extrusion (320 °C, 9:1) 3. Air cooling
HW sample	1. A sample 2. Hot extrusion (320 °C, 9:1) 3. 27 °C water cooling

3 RESULTS AND DISCUSSION

3.1 Initial microstructure

Figure 1 shows the age-hardening curve of ZK61 Mg alloy at 175 °C. As can be seen, the Vickers hardness of

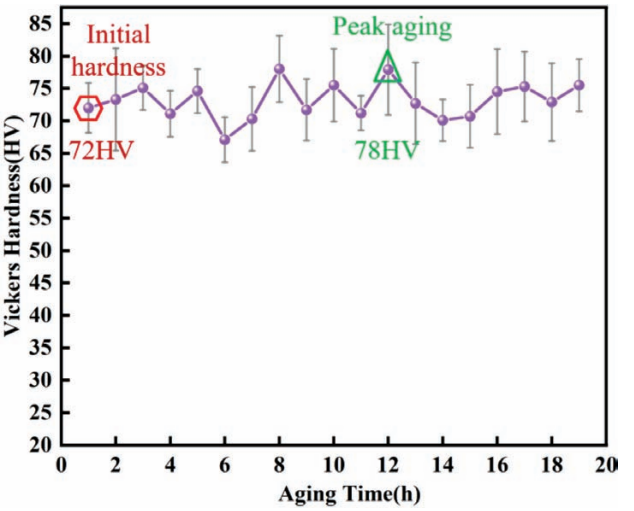

Figure 1: Age-hardening curve of ZK61 Mg alloy at 175 °C

ZK61 Mg alloy after solid solution is 72 HV, and the peak hardness of 78 HV is reached by aging the alloy at 175 °C for 12 h. A rather interesting phenomenon is found in the figure; namely, the hardness values of the alloy do not change significantly as the aging time increases. They are maintained in a range of 70–80 HV, which is quite different from the age-hardening curve of

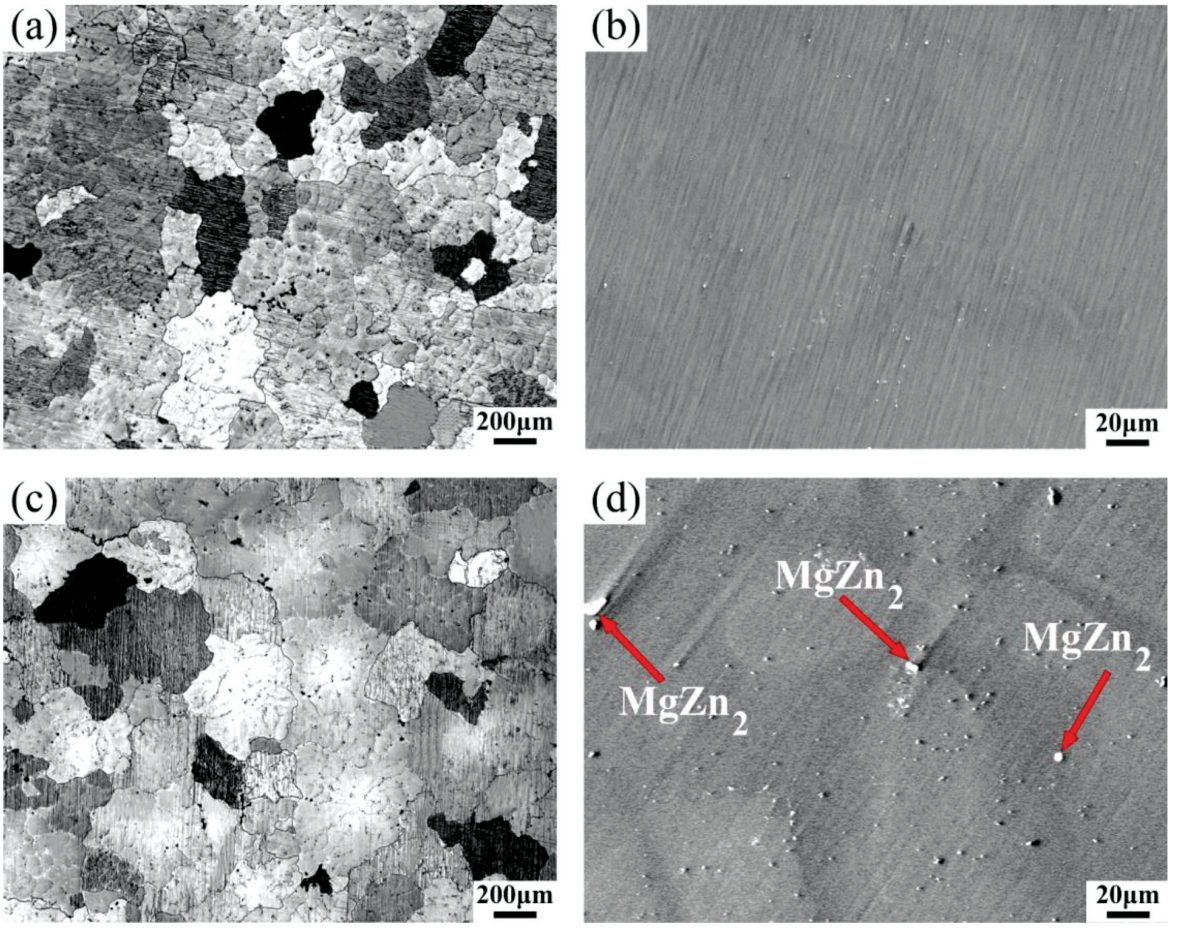

Figure 2: LM and SEM images of S sample and A sample: a, b) S sample; c, d) A sample

Mg-RE alloys where the hardness typically increases to 120–140 HV after peak aging.[27–29] From the above experimental results, it can be seen that ZK61 Mg alloy exhibits no obvious precipitation strengthening effect. This is mainly due to the low solubility of Zn in the α-Mg matrix and its low temperature sensitivity. This results in a low content of the $MgZn_2$ phase precipitated during aging, which is not sufficient to produce a significant precipitation strengthening effect.

Figure 2 shows the microstructure after homogenization and aging. **Figures 2a** and **2b** show the S sample, which was homogenized to eliminate defects such as segregation in the as-cast state. The second phase in the as-cast alloy was basically fully dissolved into the Mg matrix. **Figures 2c** and **2d** show the A sample, which was subjected to aging treatment after homogenization; its grain size was basically unchanged due to the low aging temperature. From the SEM image, it can be seen that more $MgZn_2$ phase particles[34] were precipitated after aging (shown by red arrows), affecting the DRX nucleation and grain growth in the subsequent deformation.

3.2 Microstructures at different extrusion temperatures and cooling rates

Figure 3 shows the microstructures of extruded samples. As can be seen from the OM diagrams in **Figures 3a** to **3c**, all three specimens show a binomial microstructure composed of coarse deformed grains and fine DRX grains. The coarse deformed grains are elongated along the extrusion direction, and the fine DRX grains are distributed at the grain boundaries of deformed grains. **Figures 3d** and **3g** show SEM images of the HA sample with some second phase particles uniformly distributed both at the grain boundaries and inside the grains. This is mainly due to the slow cooling rate in air after extrusion and the high driving force inside the alloy for the nucleation and growth of the second-phase particles. **Figures 3e** and **3h** show SEM images of the HW sample. Compared with the HA sample, the number of second-phase particles is obviously reduced, and most of them are distributed at the grain boundaries. The faster cooling rate caused some particles to nucleate and grow up too late, only partially nucleating at grain boundaries, dislocations and other defects. **Figures 3f** and **3i** show SEM images of the LA sample. Compared with the previous two states of the alloy, its second-phase particles are minimum and only a small amount is distributed at the grain boundaries. This is mainly due to the low deformation temperature, resulting in only a small amount of Zn entering the Mg matrix. In the subsequent cooling process, although the cooling rate is slow, it remains difficult to precipitate a fine and dispersed $MgZn_2$ phase.[30]

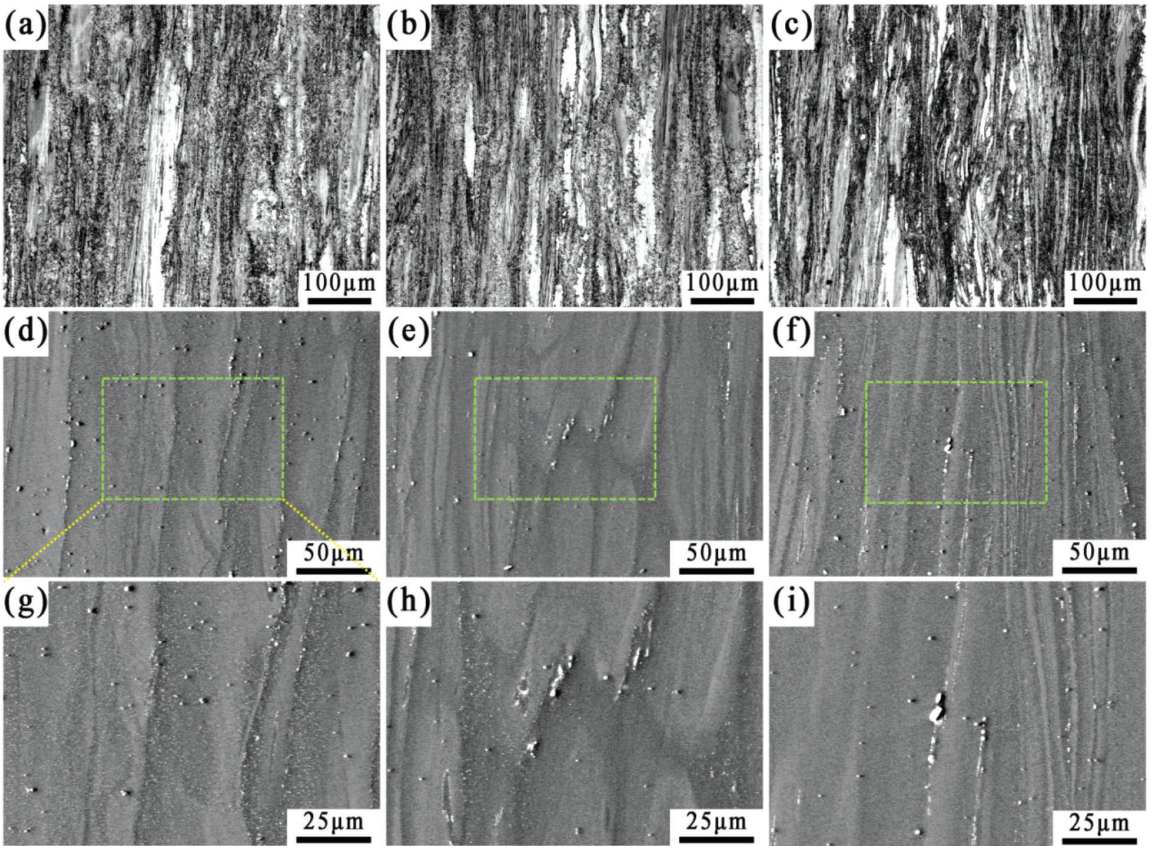

Figure 3: OM and SEM images of the extruded specimens: a, d, g) HA sample; b, e, h) HW sample; c, f, i) LA sample (where g, h, i show local magnifications of d, e, f)

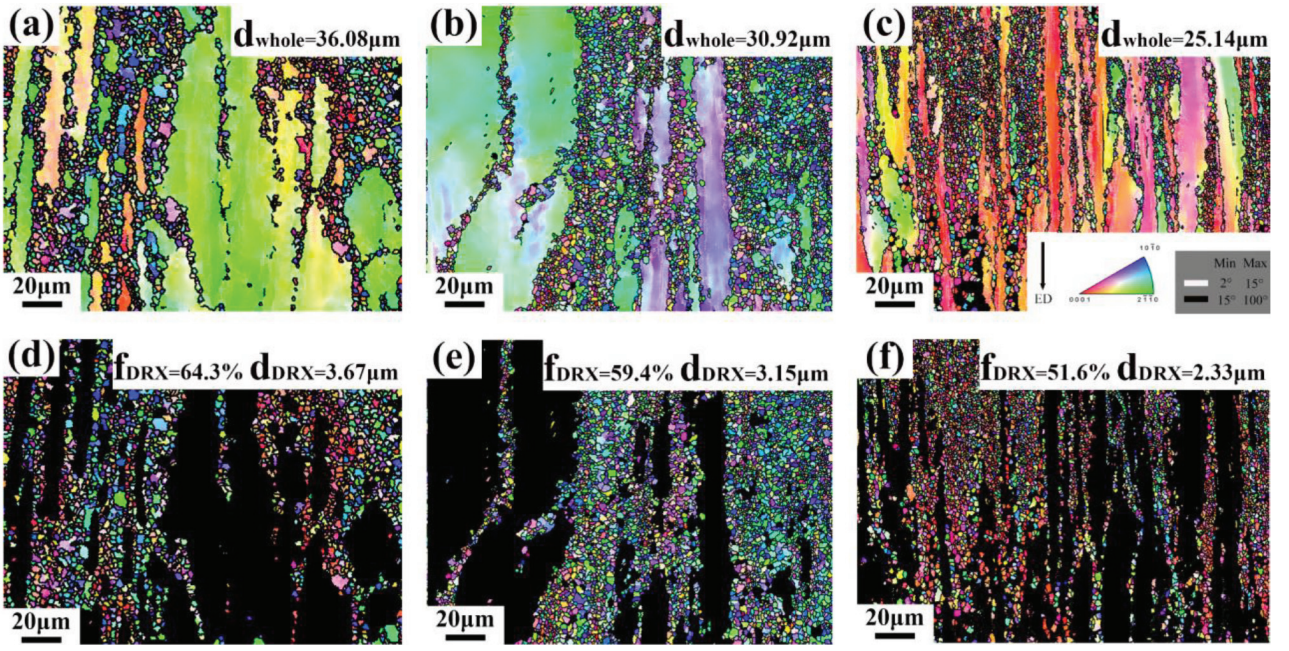

Figure 4: Corresponding IPF diagrams for the extruded specimens: a, d) HA sample; b, e) HW sample; c, f) LA sample (where a, b, c include whole grains and d, e, f include DRXed grains)

Figure 4 shows the corresponding inverse pole figures (IPFs) of the extruded samples. The observed patterns in the figure are maintained in accordance with those observed in the OM figures, and all three samples in different states show bimodal microstructures. Grain boundaries at $2 < \theta \leq 15°$are defined as low-angle grain boundaries (LAGBs) marked by white lines. In contrast, grain boundaries with $\theta > 15°$ are defined as high-angle grain boundaries (HAGBs) marked by black lines. The DRXed grains are defined as the ones with a grain orientation spread (GOS) of less than 2°.[4]

Table 2 shows the average grain sizes of the whole grains of HA sample, HW sample, and LA sample, which are (36.08, 30.92, and 25.149) μm, respectively. The DRX grains correspond to average grain sizes of (3.67, 3.15 and 2.33) μm, respectively. A comparison of the samples in three different states reveals that the HA sample has the highest DRX ratio (64.3 %), but the largest average grain size. This appears to contradict the commonly held theory that a higher DRX fraction results in finer grains. This is mainly due to the slower cooling rate after extrusion, which leads to higher internal energy after deformation, thus promoting grain-boundary migration and causing DRX grain growth. The percentage of DRX (59.4 %) and the average grain size of the HW samples do not differ much from those of the HA samples. Typically, the reason for differences in these values is mainly the growth of DRX grains during cooling. However, the overall difference in this case is small due to the limited grain growth during air cooling. The LA sample exhibits the lowest DRX percentage (51.6 %) as well as the smallest average grain size. The driving force generated during low-temperature extrusion is not sufficient for DRX, resulting in a low percentage of DRX grains. At the same time, there is no additional stored energy within the grains for grain-boundary migration, so the grains are the smallest.

Table 2: Corresponding IPF diagrams for the extruded specimens

	HA sample	HW sample	LA sample
d_{whole}	36.08 μm	30.92 μm	25.14 μm
d_{DRX}	3.67 μm	3.15 μm	2.33 μm
f_{DRX}	64.3 %	59.4 %	51.6 %

Figure 5 shows the kernel average misorientation (KAM) graphs for different specimens after extrusion. Figures a–c show distribution, while Figures d–f show distribution histograms. Different colors represent different KAM values. A KAM value increases from blue to green, and a higher KAM value represents a higher density of geometrically necessary dislocations. From plots a–c, it can be seen that fine DRXed grains are blue, while coarse deformed grains are mainly green, and green is obviously found closer to the grain boundaries. DRX is a dislocation-release process, for which dislocations provide the driving force. Dislocations move inside deformed grains during deformation. A grain boundary acts as a barrier to dislocation movement, resulting in dislocations being accumulated at the grain boundary and a larger KAM value at the grain boundary. This also explains why DRXed grains are mostly distributed at grain boundaries.

Schmid factor (SF) graphs of (0001) basal slip for different specimens after extrusion are shown in **Figure 6**. The corresponding SF values for HA, HW and LA samples are 0.20, 0.35, and 0.17, respectively. Basal slip

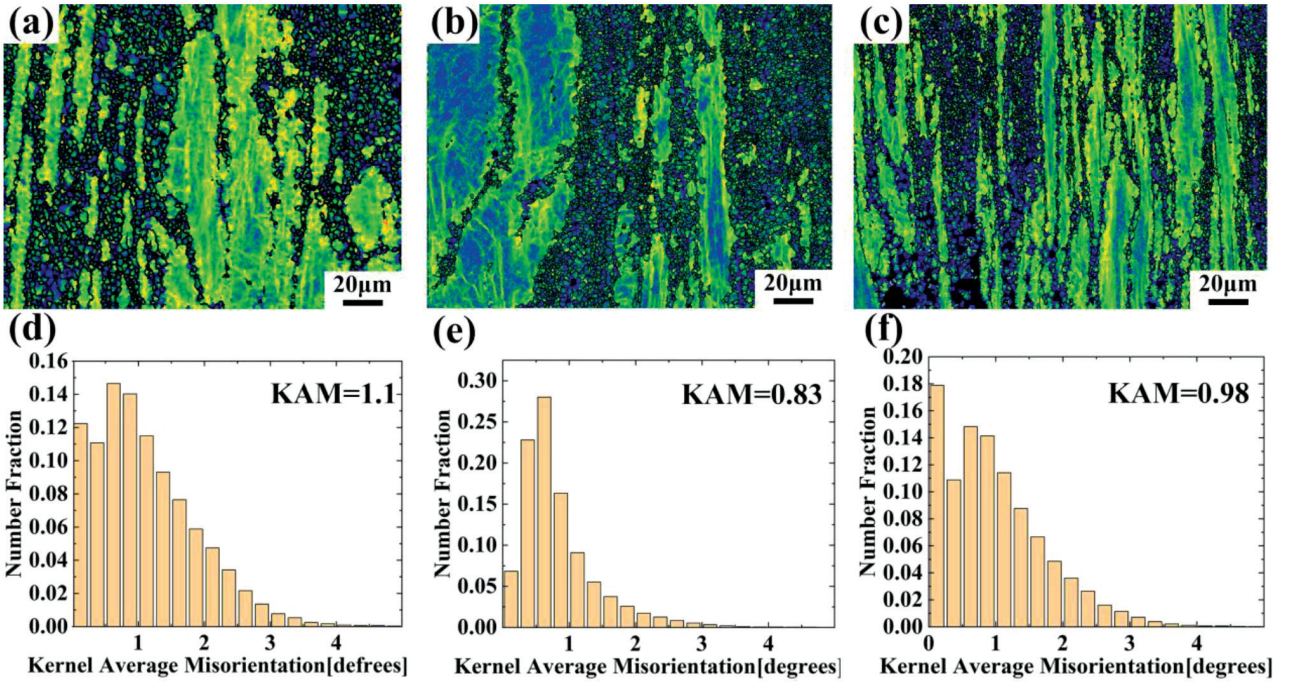

Figure 5: Corresponding KAM graphs for the extruded specimens: a, d) HA sample; b, e) HW sample; c, f) LA sample

is the main mode of slip in room-temperature deformation of Mg alloys, and the yield strength of tensile specimens is affected by the SF value.[8] From the figure, it can be seen that for the coarse deformed grains, the internal SF distribution map is mostly blue. This indicates that coarse grains do not readily undergo basal slip and are classified as hard-oriented grains. Most of the internal fine DRXed grains are orange-red, indicating that basal slip occurs readily and these are soft-oriented grains. The SF values for the HW samples are larger than those of the other samples. This may be due to the presence of more solid-solution atoms inside the deformed grains due to a faster cooling rate[35], reducing the critical shear stress (CRSS) for basal slip and making basal slip easier.

Dynamic-recrystallization mechanisms currently include two main types: continuous dynamic recrystallization and discontinuous dynamic recrystallization (DDRX). CDRX refers to the formation of dynamically

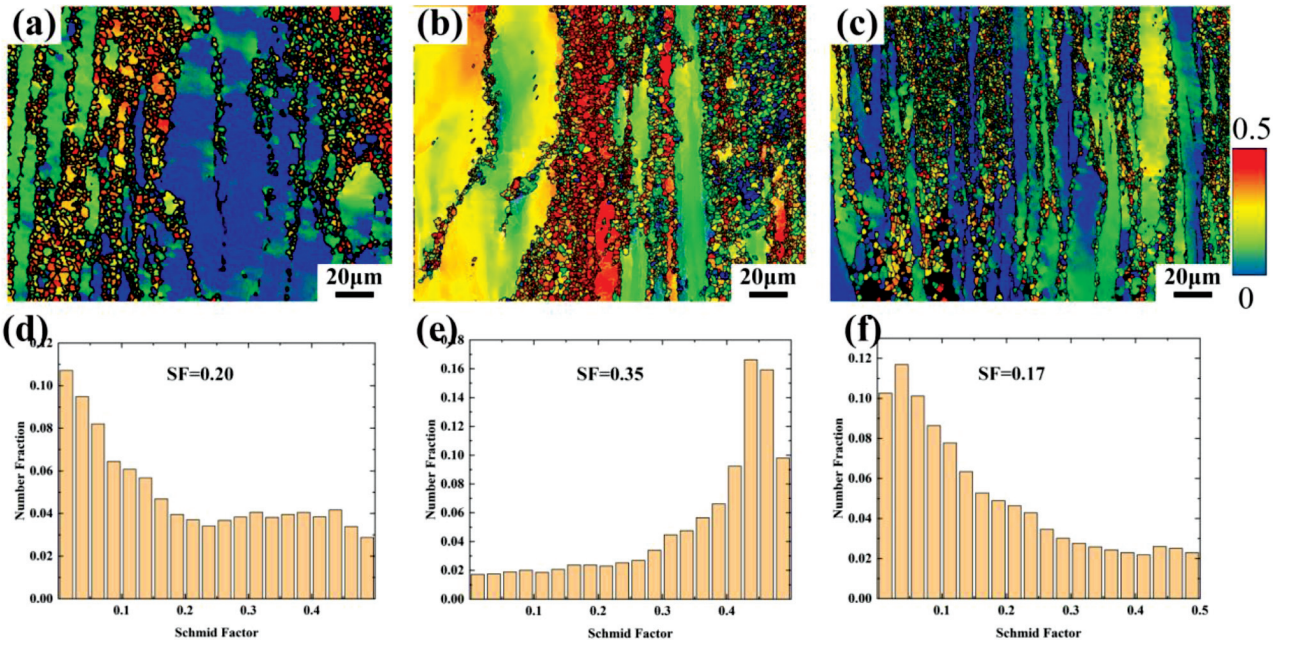

Figure 6: SF maps of (0001) basal slip for the extruded specimens: a, d) HA sample; b, e) HW sample; c, f) LA sample

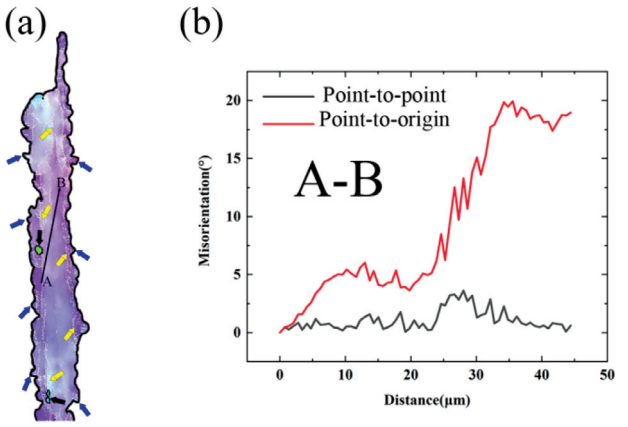

Figure 7: DRX mechanism: a) inverse pole figure map; b) line profiles of point-to-point and point-to-origin measurements along arrow AB in a)

recrystallized grains due to gradual accumulation of strain during deformation, and the transformation of low-angle grain boundaries (LAGBs) to high-angle grain boundaries (HAGBs). DDRX is the formation of nuclei at the large-angle boundaries of deformed grains, taking place through the mechanism of nucleation due to boundary bowing. DDRX refers to the nucleation of HAGB deformed grains due to the grain-boundary bow-out nucleation mechanism.[31–33]

Figure 7a shows typical grains selected in the HW sample for a more visual demonstration of the DRX mechanism. It can be seen that the edges of the selected grains are serrated (indicated by blue arrows), with the grain boundaries bowing out to the outside of the deformed grains, which is a typical feature of DDRX.[36] **Figure 7b** shows the corresponding orientation difference angle along the AB path. It can be seen that the orientation difference angle gradually increases along the path and finally reaches 20°. During deformation, strain accumulation leads to the rotation of the lattice, and the LAGBs (indicated by yellow arrows) absorbing dislocations are gradually transformed into HAGBs to form continuous dynamic recrystallized grains (indicated by black arrows).[37]

3.3 Mechanical properties

Figure 8 shows stress-strain curves of the samples in different states at RT; **Table 2** shows the corresponding tensile properties. The LA sample exhibited the best strength-plasticity synergy, with its UTS, TYS, and EL being 359.7 MPa, 281.8 MPa, and 18.8 %, respectively. There are three main reasons for this: (I) In Mg alloys, fine-grain strengthening plays a large role. According to the Hall-Petch equation ($\sigma = \sigma_0 + kd^{-\frac{1}{2}}$), a smaller average grain size corresponds to higher strength. (II) Dislocation strengthening is mainly related to the dislocation density inside the grains ($\sigma_{DIS} = \alpha MGb\sqrt{\rho}$). According to **Figure 5**, the above sample has the highest KAM value, which corresponds to higher dislocation density, and the dislocation strengthening effect is more obvious. (III) The texture strengthening is mainly attributed to the strong texture of the basal plane, which can be calculated using the SF factor of basal plane slip ($\sigma_{Tex} = \tau / m$). According to **Figure 6**, the LA sample exhibits the lowest SF value, and the texture strengthening effect is more obvious. In summary, the LA sample exhibits the best strength plasticity, mainly as a result of the combined effect of fine-grain strengthening, dislocation strengthening, and texture strengthening. The HA sample exhibits better elongation (18.0 %), but poorer strength. As can be seen in **Figure 4**, the HA sample has the largest proportion of DRX and a strong ability to accommodate dislocations, resulting in higher plasticity.

Table 2: Tensile properties of different specimens at RT

Sample type	UTS/MPa	TYS/MPa	EL/%
HA sample	282.9	209.5	18.0
HW sample	323.6	275.9	14.2
LA sample	359.7	281.8	18.8

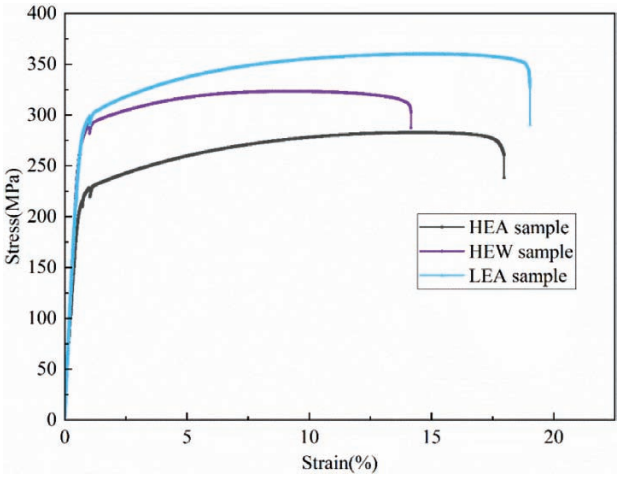

Figure 8: Stress-strain curves for samples in different states at RT

4 CONCLUSIONS

This study mainly investigated the effects of extrusion temperature and subsequent cooling modes on the microstructure and mechanical properties of ZK61 pre-aged extruded alloy. The microstructure evolution pattern and DRX mechanism were explored, and the strength-plasticity mechanism was analyzed. The results are listed below.

The microstructures of all three samples (HA, HW, LA) are bimodal, consisting of coarse deformed grains and fine DRX grains. Their average grain sizes were (3.67, 3.15, and 2.33) μm, respectively. Their DRX fractions were (64.3, 59.4, and 51.6) %, respectively.

The DRX mechanism is mainly a synergistic action of CDRX and DDRX. The higher the extrusion temperature, the higher the DRX ratio and the larger the grain

size. A higher temperature provides energy for grain-boundary migration. The faster the cooling rate, the fewer the precipitated phases, the lower the DRX fraction, and the finer the grain size. Faster cooling rates do not allow enough time for precipitates to nucleate, and DRX grains do not have the time to grow.

The LA sample showed the best strength-plasticity synergy. Its ultimate tensile strength, yield strength, and elongation were 359.7 MPa, 281.8 MPa, and 18.8 %, respectively. This was mainly the result of a combined effect of fine-grain strengthening, dislocation strengthening, and texture strengthening.

Acknowledgment

This work was supported by the Natural Science Foundation of China under grant number 52075501.

5 REFERENCES

[1] X. Wang, Y. Wang, C. Ni, Y. Fang, X. Yu, P. Zhang, The effect of T4 and T6 heat treatments on dynamic impact behavior of casting Mg-Gd-based alloys, Vacuum, 205 (**2022**), doi:10.1016/j.vacuum.2022.111450

[2] D. Deng, R. Cheng, B. Jiang, M. Yang, H. Wang, Y. Zhou, C. Yu, Y. Ma, J. Peng, F. Pan, Investigation on the microstructure evolution of high strength and ductility of as-cast Mg-9.5Gd-2.3Y-1Zn-0.5Zr alloy via double peak-aging, Nano Materials Science, 968 (**2023**), doi:10.1016/j.msea.2021.142545

[3] M. Meng, G. Lei, H. Zhang, X. Zhang, J. Yu, Precipitate characteristics and precipitation strengthening mechanism of Mg-13Gd-4Y-2Zn-0.6Zr alloy, Journal of Materials Research and Technology, 23 (**2023**), doi:10.1016/j.jmrt.2023.02.142

[4] L. Liu, B. Dong, M. Cheng, Y. Xue, Z. Zhang, Investigation of the optimum preheating treatment parameters for extruded Mg-Gd-Y-Zn-Zr alloy using high-throughput experiments, Journal of Materials Research and Technology, 25 (**2023**), doi:10.1016/j.jmrt.2023.06.230

[5] L. Liu, X. Zhou, S. Yu, J. Zhang, X. Lu, X. Shu, Z. Su, Effects of heat treatment on mechanical properties of an extruded Mg-4.3Gd-3.2Y-1.2Zn-0.5Zr alloy and establishment of its Hall–Petch relation, Journal of Magnesium and Alloys, 10 (**2022**), doi:10.1016/j.jma.2020.09.023

[6] X. Jin, W. Xu, D. Shan, B. Guo, B. Jin, Mechanism of high-strength and ductility of Mg-RE alloy fabricated by low-temperature extrusion and aging treatment, Materials & Design, 199 (**2021**), doi:10.1016/j.matdes.2020.109384

[7] K. Shi, S. Li, Z. Yu, B. Du, K. Liu, W. Du, Microstructure and mechanical performance of Mg-Gd-Y-Nd-Zr alloys prepared via pre-annealing, hot extrusion and ageing, Journal of Alloys and Compounds, 931 (**2023**), doi:10.1016/j.jallcom.2022.167476

[8] S. Hu, Q. Huo, C. Wang, T. Chen, S. Li, X. Yang, Effect of prior heat treatment on the microstructure evolution and creep resistance of ZK60 Mg alloy under tensile creep loading along normal direction, Materials Science & Engineering A, 868 (**2023**), doi:10.1016/j.msea.2023.144771

[9] M. Chen, C. Ma, Q. Liu, M. Cheng, H. Wang, X. Hu, Plastic Deformation Mechanism of High Strength and Toughness ZK61 Magnesium Alloy Plate by Multipass Horizontal Continuous Rolling, Materials, 16 (**2023**), doi:10.3390/ma16031320

[10] J. Tang, L. Chen, Z. Li, B. Que, G. Zhao, C. Zhang, Suppressing abnormal grain growth and switching precipitation behaviors in ZK60 Mg profile by inducing pre-tension, Journal of Materials Science & Technology, 155 (**2023**), doi:10.1016/j.jmst.2022.12.077

[11] S. Liu, W. Wang, X. Chen, G. Huang, H. Liu, A. Tang, B. Jiang, F. Pan, Enhanced strength and ductility AZ91 alloy with heterogeneous lamella structure prepared by pre-aging and low-temperature extrusion, Materials Science & Engineering A., 812 (**2021**), doi:10.1016/j.msea.2021.141094

[12] W. Cheng, L. Tian, H. Wang, L. Bian, H. Yu, Improved tensile properties of an equal channel angular pressed (ECAPed) Mg-8Sn-6Zn-2Al alloy by prior aging treatment, Materials Science & Engineering A., 687 (**2017**), doi:10.1016/j.msea.2017.01.054

[13] S. Liu, J. Zhang, H. Yang, X. Chen, G. Huang, A. Tang, X. Chen, B. Jiang, F. Pan, Optimization in strength-ductility of heterogeneous Mg-13Gd alloy via small extrusion ratio combined with pre-aging, Materials Science & Engineering A, 833 (**2022**), doi:10.1016/j.msea.2021.142540

[14] B. Che, L. Lu, Z. Wu, H. Zhang, M. Ma, J. Luo, H. Zhao, Dynamic recrystallization behavior and microstructure evolution of a new Mg-6Zn-1Gd-1Er alloy with and without pre-aging treatment, Materials Characterization, 181 (**2021**), doi:10.1016/j.matchar.2021.111506

[15] J. Zheng, Z. Chen, Z. Yan, Z. Zhang, Q. Wang, Y. Xue, Preparation of ultra-high strength Mg-Gd-Y-Zn-Zr alloy by pre-ageing treatment prior to extrusion, Journal of Alloys and Compounds, 894 (**2022**), doi:10.1016/j.jallcom.2021.162490

[16] K. Wang, X. Dou, J. Wang, Y. Huang, S. Gavras, N. Hort, S. Liu, H. Hu, J. Wang, F. Pan, Achieving enhanced mechanical properties in Mg-Gd-Y-Zn-Mn alloy by altering dynamic recrystallization behavior via pre-ageing treatment, Materials Science & Engineering A, 790 (**2020**), doi:10.1016/j.msea.2020.139635

[17] L. Wang, Z. Zhang, H. Zhang, H. Wang, K. Shin, The dynamic recrystallization and mechanical property responses during hot screw rolling on pre-aged ZM61 magnesium alloys, Materials Science & Engineering A, 798 (**2020**), doi:10.1016/j.msea.2020.140126

[18] C. Li, H. Liu, Y. Xin, B. Guan, G. Huang, P. Wu, Q. Liu, Achieving ultra-high strength using densely ultra-fine LPSO phase, Journal of Materials Science & Technology, 129 (**2022**), doi:10.1016/j.jmst.2022.04.036

[19] Q. Wei, L. Yuan, X. Ma, M. Zheng, D. Shan, B. Guo, Strengthening of low-cost rare earth magnesium alloy Mg-7Gd-2Y–1Zn-0.5Zr through multi-directional forging, Materials Science & Engineering A, 831 (**2022**), doi:10.1016/j.msea.2021.142144

[20] H. Wang, D. Zhang, C. Qiu, W. Zhang, D. Chen, Achieving superior mechanical properties in a low-alloyed magnesium alloy via low-temperature extrusion, Materials Science & Engineering A, 851 (**2022**), doi:10.1016/j.msea.2022.143611

[21] S. Luo, N. Wang, Y. Wang, J. Chen, H. Qin, S. Kong, T. Bai, W. Lu, L. Xiao, X. Ma, X.Yang, J. Zhang, Texture, microstructure and mechanical properties of an extruded Mg-10Gd-1Zn-0.4Zr alloy: Role of microstructure prior to extrusion, Materials Science & Engineering A, 849 (**2022**), doi:10.1016/j.msea.2022.143476

[22] W. Chen, J. Ma, C. Cui, W. Zhang, W. Wang, X. Liu, J. Yang, G. Cui, Texture role in the mechanical property improvement contributed by grain refinement for Mg-2.6Nd-0.55Zn-0.5Zr alloy subjected to extrusion process, Materials Science & Engineering A, 831 (**2022**), doi:10.1016/j.msea.2021.142185

[23] S. Liu, H. Liu, B. Zhang, G. Huang, X. Chen, A. Tang, B. Jiang, F. Pan, Effects of extrusion temperature on microstructure evolution and mechanical properties of heterogeneous Mg-Gd alloy laminates via accumulated extrusion bonding, Trans. Nonferrous Met. Soc. China, 32 (**2022**), doi:10.1016/s1003-6326(22)65940-5

[24] C. Tang, J. Chen, X. Ma, W. Liu, H. Xie, M. Li, X. Liu, Effects of extrusion speed on the formation of bimodal-grained structure and mechanical properties of a Mg-Gd-based alloy, Materials Characterization, 189 (**2022**), doi:10.1016/j.matchar.2022.111952

[25] K. Wang, J. Wang, S. Huang, X. Dou, J. Wang, C. Wang, Formation of an abnormal texture in Mg-Gd-Y-Zn-Mn alloy and its effect on mechanical properties by altering extrusion parameters, Materials Science & Engineering A, 831 (**2022**), doi:10.1016/j.msea.2021.142270

[26] T. Zhao, Y. Hu, C. Zhang, B. He, T. Zheng, A. Tang, F. Pan, Influence of extrusion conditions on microstructure and mechanical properties of Mg-2Gd-0.3Zr magnesium alloy, Journal of Magnesium and Alloys, 10 (**2022**), doi:10.1016/j.jma.2020.06.019

[27] J. Teng, X. Gong, Y. Li, Y. Nie, Influence of aging on twin boundary strengthening in magnesium alloy, Materials Science & Engineering A, 715 (**2018**), doi:10.1016/j.msea.2017.12.110

[28] J. Zheng, Z. Yan, J. Ji, Y. Shi, H. Zhang, Z. Zhang, Y. Xue, Effect of heat treatment on mechanical properties and microstructure evolution of Mg-9.5Gd-4Y-2.2Zn-0.5Zr alloy, Journal of Magnesium and Alloys, 10 (**2022**), doi:10.1016/j.jma.2021.05.018

[29] J. Wang, C. Liu, S. Jiang, G. Zeng, Effect of heat treatment on the microstructure and mechanical properties of a multidirectionally forged Mg-Gd-Y-Zn-Zr-Ag alloy, Journal of Magnesium and Alloys, 24 (**2023**), doi:10.1016/j.jma.2021.08.037

[30] S. Lv, Q. Yang, X. Lv, F. Meng, X. Qiu, Effects of reduced extrusion temperature on microstructure and mechanical properties of Mg–6Zn–0.5Zr alloy, Materials & Design, 225 (**2023**), doi:10.1016/j.matdes.2022.111568

[31] C. Liu, L. Liu, J. Zheng, Z. Yan, Z. Zhang, Q. Wang, X. Li, Y. Xue, Effect of Annealing Before Aging on Microstructure and Mechanical Properties of Mg-Gd-Y-Zn-Zr Alloy, Journal of Materials Engineering and Performance, (**2022**), doi:10.1007/s11665-022-07022-w

[32] C. Liu, J. Ji, J. Zheng, Q. Wang, Z. Zhang, Y. Xue, Microstructure evolution and mechanical properties of cup-shaped specimens prepared by rotary backward extrusion, Journal of Materials Research and Technology, 23 (**2023**), doi:10.1016/j.jmrt.2023.01.029

[33] S. Liu, H. Liu, X. Chen, G. Huang, Q. Zou, A. Tang, B. Jiang, Y. Zhu, F. Pan, Effect of texture on deformation behavior of heterogeneous Mg-13Gd alloy with strength–ductility synergy, Journal of Materials Science & Technology, 113 (**2022**), doi:10.1016/j.jmst.2021.09.0 65

[34] J. Zheng, L. Liu, W. Liu, Y. Huang, Z. Zhang, Q. Wang, Z. Yan, Y. Xue, Effect of heterogeneous microstructure on the mechanical properties and deformation behavior of rotating backward extruded ZK61 alloy, Journal of Alloys and Compounds, 926 (**2022**), doi:10.1016/j.jallcom.2022.166920

[35] P. Peng, K. Zhang, J. She, A. Tang, J. Zhang, K. Song, Q. Yang, F. Pan, Role of second phases and grain boundaries on dynamic recrystallization behavior in ZK60 magnesium alloy, Journal of Alloys and Compounds, 861 (**2021**), doi:10.1016/j.jallcom.2020.157958

[36] L. Liu, X. Zhou, S. Yu, J. Zhang, X. Z. Lu, X. Shu, Z. J. Su, Dissolution and reprecipitation of 14H-LPSO structure accompanied by dynamic recrystallization in hot-extruded Mg89Y4Zn2Li5alloy, J. Magnes. Alloys, (**2022**), doi:10.1016/j.jma.2020.09.023